Magnetic behavior of the Ni$_x$Fe$_{1-x}$Nb$_2$O$_6$ quasi-one-dimensional system: Isolation of Ising chains by frustration

P. W. C. Sarvezuk,[1,2] M. A. Gusmão,[1] J. B. M. da Cunha,[1] and O. Isnard[2,*]

[1]*Instituto de Física, Universidade Federal do Rio Grande do Sul, C.P. 15051, 91501-970 Porto Alegre, Brazil*
[2]*Institut Néel, CNRS and Université Joseph Fourier, B.P. 166, 38042 Grenoble Cedex 9, France*

Physical properties of the Ni$_x$Fe$_{1-x}$Nb$_2$O$_6$ compounds are investigated combining x-ray and neutron powder diffraction with magnetic and calorimetry measurements as well as ^{57}Fe Mössbauer spectroscopy. This system is known to present quasi-one-dimensional magnetism with the magnetic moments arranged along weakly interacting Ising chains. Partial substitution of the magnetic ion tends to suppress the magnetic ordering observed in the end members of the series. When this happens, the low-temperature magnetic specific heat agrees well with what is expected for isolated Ising chains. The lowest temperature powder neutron-diffraction patterns exhibit evidence for the occurrence of short-range order, and analysis of these diffuse neutron-scattering patterns allow us to obtain information on the magnetic correlations. The suppression of magnetism is consistently interpreted as resulting from the magnetic-cation disorder induced by substitution, which enhances the system's tendency for frustration of geometrical origin.

PACS number(s): 75.25.−j, 75.30.Cr, 75.50.Ee

I. INTRODUCTION

The characteristics of low dimensionality in compounds of the type MX_2O_6 (M = Mn, Fe, Co, Ni; X = Ta, Nb) have been extensively investigated. While the tantalites are tetragonal and present quasi-two-dimensional magnetic properties, the niobates are orthorhombic and characterized by quasi-one-dimensional magnetism[1–3] besides presenting interesting optical and dielectric properties.[4–7] The MNb$_2$O$_6$ compounds present the *Pbcn* orthorhombic space group,[1,2] known as columbite structure. In this structure, the M^{2+} and Nb^{5+} cations are located at 4c and 8d positions, respectively. A sketch of the unit cell is shown in Fig. 1. The oxygen atoms sit on three nonequivalent positions so that the stacking of oxygen octahedra surrounding the cations form zigzag chains along the c axis, with the octahedra slightly tilted away from this axis. The zigzag chains are characteristic of the α-PbO$_2$ structure.[8,9] The octahedra surrounding the M^{2+} and the Nb^{5+} cations are both quite distorted. This structure can alternatively be described as resulting from layers of distorted octahedra forming a hexagonal closed-packed lattice. These layers are perpendicular to the orthorhombic a axis in the following sequence of cations: M-Nb-Nb-M-Nb-Nb-M.

Previous investigations of the FeNb$_2$O$_6$ and NiNb$_2$O$_6$ compounds have pointed out the existence of (partial) geometrical frustration among the exchange interactions, due to an isosceles-triangle coordination on the ab planes. This leads to interesting magnetic behavior influenced by a few different exchange couplings. NiNb$_2$O$_6$ and FeNb$_2$O$_6$ present a transition from the paramagnetic phase to an ordered spin structure[10] at 5.7 and 4.9 K, respectively.[1] The magnetism in FeNb$_2$O$_6$ has been studied first by Weitzel,[10] who reported a collinear magnetic structure with propagation vector (0,1/2,0) for FeNb$_2$O$_6$. A noncollinear canted structure has later been suggested based on magnetization measurements as well as group theoretical considerations.[11,12] The magnetic phase diagram for nickel and iron columbites has been reinvestigated by Heid *et al.*,[1,2] who showed that both FeNb$_2$O$_6$ and NiNb$_2$O$_6$ exhibit antiferromagnetic order with a canted magnetic structure. They also established the presence of two phases, with propagation vectors, (0,1/2,0) and (1/2,1/2,0), on the basis of magnetic measurements combined with neutron diffraction carried out on both powder samples and single crystals.

In this paper, we report on the evolution of the structural and magnetic properties with transition-metal composition on six powder samples within the Ni$_x$Fe$_{1-x}$Nb$_2$O$_6$ series. Our main focus is on the stability of the ordered magnetic phases upon magnetic-cation substitution. We find that magnetic ordering, although present in the end members of the series, tends to be suppressed even for small amounts of cation substitution. The system, then, approaches the behavior of a collection of isolated Ising chains, although evidence of short-range order is clearly present, mainly in the neutron-diffraction patterns.

The paper is organized as follows. Section II is devoted to the description of the experimental techniques used. The main results are reported in Sec. III, divided in discussions of structural characteristics (see Sec. III A), specific-heat behavior with temperature (see Sec. III B), magnetic measurements, including susceptibility and magnetization curves (see Sec. III C), and Mössbauer spectra (see Sec. III D). Section IV presents a summary of the main results and conclusions.

II. EXPERIMENTAL

Powder samples were prepared with appropriate amounts of Fe$_2$O$_3$, powder metallic Fe and Nb$_2$O$_5$ for FeNb$_2$O$_6$ and NiO and Nb$_2$O$_5$ for NiNb$_2$O$_6$. The mixtures were ground, pressed to pellets and heat treated in vacuum for FeNb$_2$O$_6$ and in air for NiNb$_2$O$_6$, respectively, at 1370 K for 24 h and 1570 K for 30 h. Then stoichiometric amounts of FeNb$_2$O$_6$ and NiNb$_2$O$_6$ were mixed, regrinded and heat treated for 24 h in vacuum at 1570 K. The obtained samples were slowly cooled and powdered with grain size below 44 microns. Powder of Ni$_x$Fe$_{1-x}$Nb$_2$O$_6$ was prepared by mixing approprieted amounts of FeNb$_2$O$_6$ and NiNb$_2$O$_6$ and submitting the mixture to the same heat treatment in vacuum. The samples were found to be stable
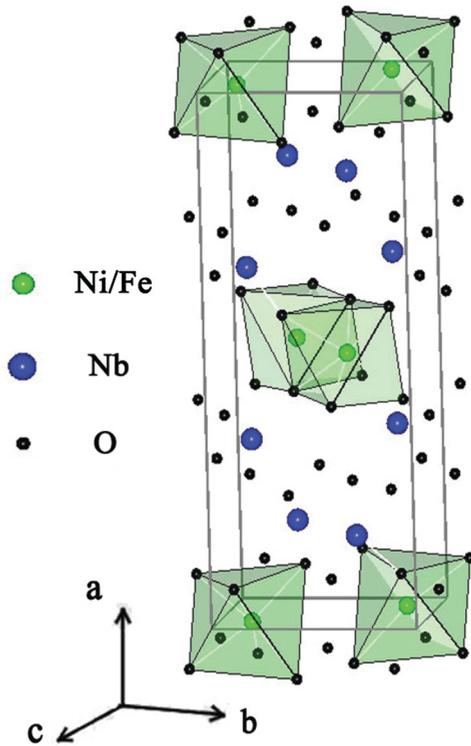
FIG. 1. (Color online) Unit cell of the MNb$_2$O$_6$ structure, showing the oxygen octahedra surrounding the magnetic cations.

in air at ambient condition since the x-ray pattern has been found to be identical after several months. A large amount of sample, at about 2.5 g, was prepared for the neutron diffraction measurements (ND).

The sample purity was first checked by x-ray diffraction (XRD) analysis before carrying out studies of magnetic properties. Such XRD analysis was performed in the Bragg-Brentano geometry, using CoKα radiation, λ(Kα_1) = 1.540 56 Å and λ(Kα_2) = 1.544 39 Å, with scan step 0.05° and angular 2θ range from 10° to 80°.

Specific-heat measurements were performed with an ac calorimeter, at temperatures ranging from 1.8 to 44 K, using the physical property measurement system (PPMS-14, Quantum Design) installed at Institut Néel (France). The relaxation 2τ fitting method was used for the measurement. The masses of the samples were in the range of 5–9 mg. These measurements were made with the aim of investigating the existence of a magnetic phase transition through the sharp peak usually observed in the molar specific heat C_m at the Néel temperature.

The magnetic properties were measured in a wide temperature range, from 1.7 to 300 K. The measurements were carried out using the extraction method and an experimental set up that has been described elsewhere.[13] Both isothermal magnetization and susceptibility as a function of temperature were measured. The isothermal magnetization curves were recorded at magnetic fields in the range corresponding to $\mu_0 H$ = 0 to 10 T, while the temperature-dependent magnetic susceptibility $\chi(T)$ was measured at $\mu_0 H$ = 0.5 T.

Neutron-diffraction measurements were carried out on powder samples. The data were collected with the double-axis multicounter high-flux diffractometer D1B operated by the CNRS at the Institut Laue Langevin (ILL), Grenoble, using 2.52 Å wavelength selected by a pyrolitic graphite monochromator. D1B is a powder diffractometer operating with the takeoff angle of the monochromator at 44° (in 2θ). In the configuration used, the resolution of D1B was about 0.3° (full width at half maximum) and the multicounter was composed of 400 cells covering a total angular domain of 80°. The angular 2θ range was from 5° to 85° with a detector step of 0.2°.

X-ray and neutron-diffraction data analysis was done using the FULLPROF refinement package[14] in order to extract the crystallographic parameters. Agreement factors used in this article are defined according to the guidelines of the Rietveld refinement that can be found elsewhere.[15] The neutron scattering lengths used were 0.7054×10^{-12} cm for Nb, 0.9450×10^{-12} cm for Fe, 1.03×10^{-12} cm for Ni, and 0.5803×10^{-12} cm for O, values taken from Sears.[16]

Fe Mössbauer spectroscopy (MS) is an adequate technique to investigate order-disorder transitions in this kind of materials. Hyperfine interactions are very sensitive to change in the neighboring environment and can discriminate site location of Fe ions in columbite-like samples.[17] For the Mössbauer spectroscopy measurements, absorbers with 50 mg of ground (below 44 microns) material were prepared in order to satisfy the ideal absorber thickness approximation.[18] The spectra were obtained at room temperature, using a constant acceleration electromechanical drive system with a multichannel analyzer for collecting and storing the data. The hyperfine parameters were obtained by a least-squares fitting assuming Lorentzian line shapes. ^{57}Co in rhodium was used as source, with nominal activity of 50 mCi. A high-purity Fe metal foil was used for velocity scale calibration.

III. RESULTS AND DISCUSSION

A. Crystal structure

The (Fe,Ni)Nb$_2$O$_6$ compounds were found to be single phase according to the analysis of the x-ray diffraction patterns. This analysis confirms that the *Pbcn* space-group symmetry is retained for all the studied compounds. The lattice parameters were obtained from x-ray and neutron-diffraction data, recorded at room temperature and 20 K, respectively. The obtained values are summarized in Table I, where we can see that the composition dependence of the unit-cell volume at both temperatures confirms the existence of a solid solution in the whole composition range. The Fe for Ni substitution is found to induce an increase of the unit-cell volume, the rate of increase being essentially the same at high and low temperatures. Furthermore, as expected, the unit-cell volume is slightly smaller at low temperature. As an example of the Rietveld analysis, x-ray and neutron diffraction patterns are shown in Fig. 2 for Ni$_{0.2}$Fe$_{0.8}$Nb$_2$O$_6$. The unit cell is found to evolve anisotropically: both the a and b parameters increase continuously with the Fe concentration, but a is much more sensitive to the Fe content, while c is much less affected by composition changes. This may indicate that the value of c is mainly determined by the NbO$_6$ octahedra rather than by the (Fe,Ni)O$_6$ ones.

As can be seen from the fitted diffraction patterns given in Fig. 2, the room-temperature crystal-structure symmetry

TABLE I. Composition dependence of unit-cell parameters along the $\mathrm{Ni}_x\mathrm{Fe}_{1-x}\mathrm{Nb}_2\mathrm{O}_6$ series at room temperature (x rays) and 20 K (neutrons).

x		1.0	0.8	0.6	0.4	0.2	0.0
a (Å)	X rays	14.031(3)	14.078(1)	14.123(1)	14.171(1)	14.217(3)	14.258(2)
	Neutrons	14.021(1)	14.050(2)	14.090(4)	14.163(1)	14.212(1)	14.251(1)
b (Å)	X rays	5.681(1)	5.693(2)	5.704(2)	5.714(3)	5.723(2)	5.731(1)
	Neutrons	5.675(1)	5.693(1)	5.691(2)	5.699(2)	5.720(1)	5.722(2)
c (Å)	X rays	5.021(2)	5.028(4)	5.034(1)	5.038(2)	5.043(2)	5.046(2)
	Neutrons	5.022(1)	5.027(1)	5.028(1)	5.028(2)	5.034(2)	5.035(1)
Volume (Å)^3	X rays	400.2(2)	403.0(3)	405.5(1)	408.0(1)	410.4(2)	412.3(2)
	Neutrons	399.5(3)	402.1(1)	403.3(3)	405.9(1)	409.3(2)	410.5(2)

is preserved at 20 K. This is also true at 1.7 K. Indeed, refinement of the diffraction patterns demonstrates that the crystal structure is kept down to 1.7 K for all the investigated compounds, and no change of symmetry is observed. The positions of the oxygen atoms were confirmed by neutron diffraction, which is known to be more sensitive to the position of light elements than x-ray diffraction. In order to investigate the magnetic structure, low-temperature neutron diffraction patterns were recorded at 1.7 K for all the synthesized compositions.

Table II summarizes the atomic-position parameters for two typical compositions: $\mathrm{Ni}_{0.8}\mathrm{Fe}_{0.2}\mathrm{Nb}_2\mathrm{O}_6$ and $\mathrm{Ni}_{0.2}\mathrm{Fe}_{0.8}\mathrm{Nb}_2\mathrm{O}_6$. Similar values were found for the other studied compounds, indicating that there is little change of the crystal structure upon Fe for Ni replacement. The low-temperature neutron-diffraction patterns do not exhibit extra reflexions that could be attributed to magnetic order. A difference pattern has been calculated by subtracting the pattern recorded at 20 K from that recorded at 1.7 K. Figure 3 shows that this difference pattern exhibits a broad signal around 12.3° in 2θ but no magnetic

Bragg reflections, confirming that at 1.7 K the sample is not ordered magnetically. Similar results were obtained for all the mixed compositions. The presence of such broad signal of magnetic origin is indicative of short-range order (SRO). Such SRO could result from the proximity of a magnetic transition at a lower temperature. To check this possibility, further neutron diffraction at very low temperature was necessary. To do so, we focused our investigation on the $\mathrm{Ni}_{0.2}\mathrm{Fe}_{0.8}\mathrm{Nb}_2\mathrm{O}_6$ sample, recording neutron-diffraction patterns at several temperatures down to 400 mK using an $^3\mathrm{He}$ cooling insert in the Orange cryostat of the Institut Laue Langevin. No transition was observed, which implies the absence of a magnetic phase, but the broad feature indicates the presence of short-range magnetic correlations. The temperature evolution of the diffraction pattern clearly shows the increase of correlations with decreasing temperature as the peak becomes sharper. It can be seen in more detail in Fig. 4, where we notice that the magnetic correlations are no longer changing with temperature around 1.0 K. In particular, the magnetic signal is nearly identical for the patterns recorded at 1.0 K and 400 mK. It is interesting to notice that the maximum of the broad SRO signal is close to the position where the (0,1/2,0) and (1/2,1/2,0) peaks are observed for the magnetic compounds $\mathrm{NiNb}_2\mathrm{O}_6$
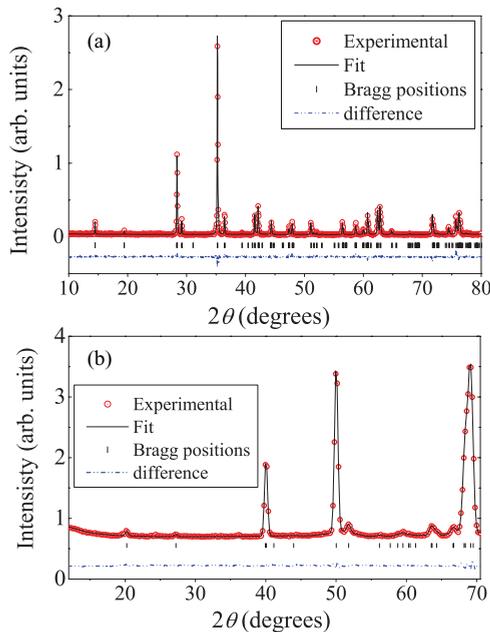
FIG. 2. (Color online) Rietveld refinement of the (a) x-ray and (b) neutron diffraction at 300 and 20 K, respectively, for $\mathrm{Ni}_{0.2}\mathrm{Fe}_{0.8}\mathrm{Nb}_2\mathrm{O}_6$.

TABLE II. Structure-refinement parameters and atomic positions (x, y, z) obtained from neutron powder diffraction data recorded at 20 K for $\mathrm{Ni}_{0.8}\mathrm{Fe}_{0.2}\mathrm{Nb}_2\mathrm{O}_6$ and $\mathrm{Ni}_{0.2}\mathrm{Fe}_{0.8}\mathrm{Nb}_2\mathrm{O}_6$.

$\mathrm{Ni}_{0.8}\mathrm{Fe}_{0.2}\mathrm{Nb}_2\mathrm{O}_6$: space group *Pbcn*, $R_{wp} = 4.08\%$, $R_B = 2.87\%$.			
Atom	x/a	y/b	z/c
Nb	0.1559(9)	0.324(5)	0.773(7)
O(1)	0.101(2)	0.388(4)	0.401(6)
O(2)	0.078(2)	0.109(5)	0.950(3)
O(3)	0.248(2)	0.116(6)	0.577(4)
Fe/Ni	0	0.177(4)	0.25
$\mathrm{Ni}_{0.2}\mathrm{Fe}_{0.8}\mathrm{Nb}_2\mathrm{O}_6$: space group *Pbcn*, $R_{wp} = 1.33\%$, $R_B = 1.43\%$.			
Atom	x/a	y/b	z/c
Nb	0.161(1)	0.3186(3)	0.759(5)
O(1)	0.095(2)	0.387(3)	0.415(3)
O(2)	0.0799(13)	0.126(7)	0.909(3)
O(3)	0.257(2)	0.1023(4)	0.577(3)
Fe/Ni	0	0.159(7)	0.25
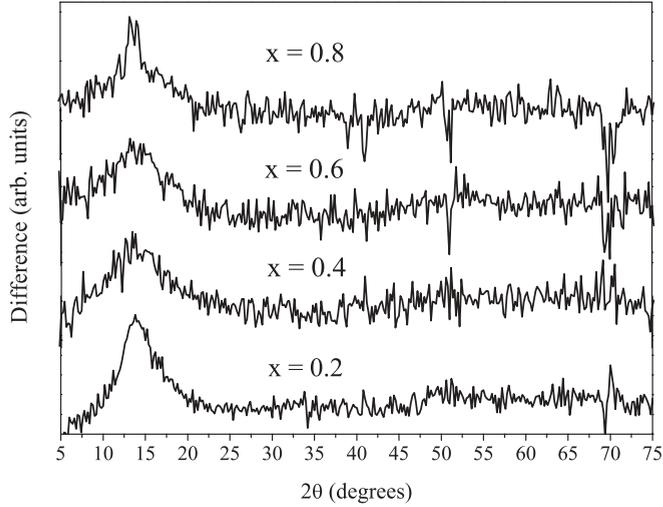
FIG. 3. Difference of the neutron powder diffraction patterns of $Ni_xFe_{1-x}Nb_2O_6$ between 20 K and 1.7 K for the quoted compositions, showing the absence of Bragg reflections and the presence of a broad peak. The curves are displaced for clarity.

and $FeNb_2O_6$. The center of the SRO peak corresponds to a $Q \approx 0.53$ Å^{-1}, and its half width is about ten times larger than the experimental resolution.

To fit the diffuse signal observed on the experimental data, we considered a description of the magnetic-scattering as due to short range spin-spin correlations, with the signal intensity described by an expression first proposed for spin glasses in Refs. 19 and 20, and applied to pyrochlores in Refs. 21 and 22,

$$ I(q) = N \left[\frac{1}{2} r_0 \gamma_0 f_m(q) \right]^2 \frac{2}{3} \sum_{i=1}^{n} c_i \gamma_i \frac{\sin(q R_i)}{q R_i} . \quad (1) $$

Here, $\frac{1}{2} r_0 \gamma_0$ is the scattering length per Bohr magneton, $f_m(q)$ is the magnetic form factor of the mean $(Fe/Ni)^{2+}$ cation, the summation is over the coordination shells surrounding
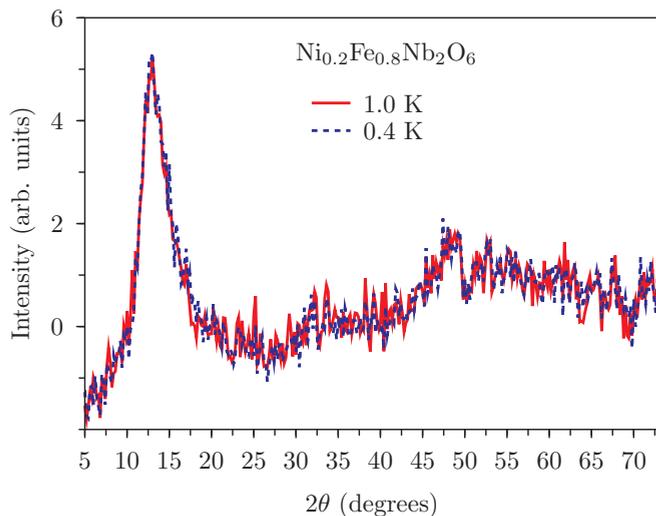
FIG. 4. (Color online) Neutron-diffraction difference signals between 20 K and the indicated temperatures for $Ni_{0.2}Fe_{0.8}Nb_2O_6$, showing that the pattern is no longer changing in this temperature range and no magnetic ordering occurs.
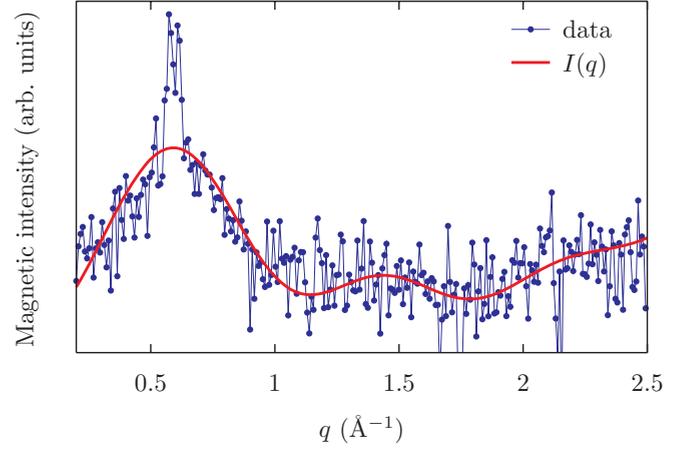
FIG. 5. (Color online) Detailed view of the diffuse neutron scattering pattern for $Ni_{0.8}Fe_{0.2}Nb_2O_6$. The line is a fitting to Eq. (2). One can see a precursor of a Bragg peak growing on top of the diffuse signal.

a central atom, c_i and R_i are, respectively, the number of neighbors and the radius of the coordination shell, known from crystallographic data, and γ_i is the average spin correlation at each bond distance.

For the $Ni_xFe_{1-x}Nb_2O_6$ compounds, we took into account distances up to 10 Å. We fitted the subtracted data with the equation

$$ I(q) = \sum_{i=1}^{n} c_i \Gamma_i \frac{\sin(q R_i)}{q R_i} + B , \quad (2) $$

where Γ_i and B are adjustable parameters. The Γ_i are proportional to the average spin-spin correlation function for each distance, absorbing all the coefficients in Eq. (1), and B is a constant background contribution. At 2 K, we obtain a good description of the diffuse scattering, correctly accounting for the intensity, position, and oscillations of the diffuse signal. An example of such fitting is given in Fig. 5, where one also observes the onset of a long-range-order peak on top of the diffuse signal. In this example, we used coordination shells of radii 3.22, 4.45, 5.02, 5.7, 7.9, 9.4 Å. The first four are actual cation-cation distances, while the latter two correspond to averages of distances in shells nearly 1 Å wide. The reason for taking the averages is that a large number of close distances does not allow for a trustful fitting with the range of available data. Besides, it is clear from Fig. 5 that the intensity variations, apart from the noise due to experimental precision, are dominated by short distances, i.e., long periods in wave vector. Similar fittings for all the studied compositions allowed us to obtain relative spin-spin correlations averaged over each coordination shell, which are listed in Table III. The distances show small variations with respect to the typical ones quoted in the table depending on the actual composition. It can be clearly seen that ferromagnetic correlations exist within the zigzag chains, corresponding to the distances 3.22 and 5.02 Å. On the other hand, the correlations between magnetic sites at distances corresponding to the shortest interchain bonds (4.45 and 5.7 Å) along the b direction are found to be antiferromagnetic whatever the composition. The last two shells in Table III involve both intrachain and interchain contributions, since they

TABLE III. Composition dependence of the magnetic correlations for the nearest atomic distances in the lattice, as derived from a fitting of the low-temperature neutron diffuse scattering signal of magnetic origin. The values are normalized to the correlations obtained for nearest neighbors.

Sample	Relative spin-spin correlation					
$Ni_{0.2}Fe_{0.8}Nb_2O_6$	1	−1.45	2.14	−1.97	−0.21	0.082
$Ni_{0.4}Fe_{0.6}Nb_2O_6$	1	−0.99	1.36	−1.47	−0.11	0.0018
$Ni_{0.6}Fe_{0.4}Nb_2O_6$	1	−0.70	1.09	−1.06	−0.12	0.051
$Ni_{0.8}Fe_{0.2}Nb_2O_6$	1	−1.65	2.21	−1.36	−0.099	0.039
Typical distances (Å)	3.22	4.45	5.02	5.7	7.9	9.4

are averages over a large number of atoms, as discussed above. We can also see that the shorter-range correlations are larger for the low-substitution compounds $Fe_{0.8}Ni_{0.2}Nb_2O_6$ and $Ni_{0.8}Fe_{0.2}Nb_2O_6$ and are clearly reduced for the intermediate compositions. This is consistent with the absence of any hint of long-range magnetic ordering in these latter cases, for which the magnetic neutron-diffraction signal (not shown) present only broad bumps.

It is interesting to remark that the two compounds at the ends of the series, $FeNb_2O_6$ and $NiNb_2O_6$, are magnetically ordered, exhibiting a mixture of two magnetic structures, described by the propagation vectors $(0,1/2,0)$ and $(1/2,1/2,0)$. However, the Fe compound show dominantly the $(0,1/2,0)$ phase (91%) whereas for the Ni compound the situation is reversed, the $(1/2,1/2,0)$ being dominant (79%) in our refinement. These results are in excellent agreement with earlier report by Heid and coworkers.[1] Ni/Fe substitutions on either of the two magnetic compounds induce the disappearance of long-range magnetic order down to very low temperature. One can speculate that the observed competition between two magnetic phases and its evolution with composition plays an important role in this suppression of long-range order. This most probably has to be attributed to chemical disorder, since the crystal structure of the studied compounds is not modified (no change of space group) throughout the $Ni_xFe_{1-x}Nb_2O_6$ series, except for a small volume change, as discussed in Sec. III A. It is worth remarking that the signs of the shorter-range correlations in Table III are in agreement with both magnetic structures. Unfortunately, the need to average over the large-distance shells does not allow us to see an evolution from dominance of one or the other.

We must also keep in mind that even the ordered compounds present competing exchange interactions due to the lattice geometry. Indeed, it has been reported[3,23,24] that in the ANb_2O_6 structure competing antiferromagnetic interactions exist within the triangular net of ferromagnetic chains, as sketched in Fig. 6. This geometrical frustration is not complete because of differences in interchain exchange couplings (J_1 and J_2 in Fig. 6). Recent theoretical calculations on the isotype compound $CoNb_2O_6$ have shown that many magnetic phase transitions may occur depending on the ratio between the exchange integrals and the presence of applied magnetic field.[25] In the series studied here, we observe that replacement of Ni by Fe leads to a change in lattice parameters such that the maximum $\Delta b/b$ is about 1.6% against only 0.9% for $\Delta a/a$. This obviously indicates anisotropic evolution of the
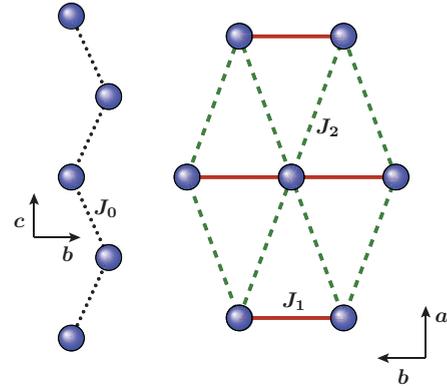
FIG. 6. (Color online) Schematic representation of a zigzag chain of magnetic ions and the triangular arrangement of the chains across the ab plane. The exchange constants within a chain (J_0) and between magnetic ions in neighboring chains (J_1 and J_2) are indicated.

interatomic distances involved in the isosceles triangular lattice characterizing the ab plane, with relevant effect on the values of the competing exchange interactions. The modification of magnetic properties most probably results from the cationic disorder induced by random substitution, with the accompanying exchange-coupling disorder. The latter can average down the above mentioned differences in interchain coupling, thus rendering effective the geometrical frustration of the triangular arrangement of ferromagnetic chains. In such case, the system may be considered as a collection of independent Ising chains, and hence not ordered at any finite temperature.

B. Specific-heat measurements

In order to further check the occurrence of a magnetic transition at low temperature, specific heat measurements were carried out down to 1.8 K for the $Ni_{0.2}Fe_{0.8}Nb_2O_6$ and $Ni_{0.6}Fe_{0.4}Nb_2O_6$ compounds. The corresponding curves are plotted in Fig. 7. No sign of magnetic ordering is found in this temperature range and no pronounced anomaly can be
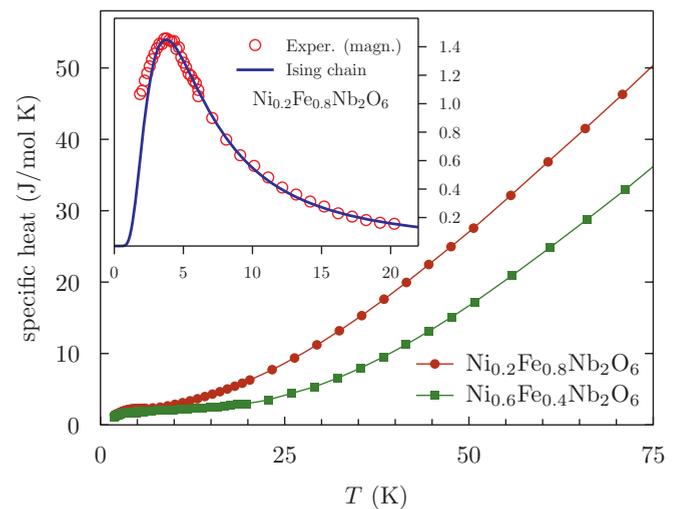
FIG. 7. (Color online) Low-temperature specific heat measurement recorded for $Ni_{0.2}Fe_{0.8}Nb_2O_6$. The inset shows a fitting of the magnetic part with the expression for an isolated Ising chain.

TABLE IV. Intrachain (J_0) and (average) interchain ($J_\perp$) exchange constants of $Ni_xFe_{1-x}Nb_2O_6$ compounds as derived from the Ising-chain specific heat (C_m) and magnetic susceptibility (χ_0).

x	1.0	0.8	0.6	0.4	0.2	0.0
J_0 (K) [C_m]	...	...	2.7	...	1.4	...
J_0 (K) [χ_0]	6.0	2.51	2.07	1.25	1.03	1.12
$J_\perp$ (K) [χ_0]	−0.35	...	...	...	...	−0.098

observed from room temperature down to about 10 K. A small but significant bump is however noticeable below 10 K. After subtracting the nonmagnetic contribution from a polynomial fitting of the behavior above 20 K, we obtained a typical low-temperature behavior as shown in the inset of Fig. 7. One can see that the magnetic specific heat is remarkably well fitted using the well-known theoretical expression for an Ising linear chain,[26]

$$C_m(T) = \left(\frac{J_0 S^2}{T}\right)^2 \text{sech}\left(\frac{J_0 S^2}{T}\right) \qquad (3)$$

(apart from a units correction factor), where J_0 is the exchange coupling along the chain, and S is the spin value, which is obtained as a simple average weighted by the concentrations of each magnetic ion, varying from $S = 2$ for Fe to $S = 1$ for Ni. The intrachain exchange constant obtained from the fitting is $J_0 = 1.4$ K for $x = 0.2$. The same procedure was also applied to $Ni_{0.6}Fe_{0.4}Nb_2O_6$. The exchange values are listed in Table IV, in comparison with those obtained from the magnetic susceptibility (see Sec. III C). As can be seen in the inset of Fig. 7, the data starts to depart from the fitted curve at the lowest temperatures, which may be an indication of correlations occurring between the chains in this temperature range. This is consistent with our previous discussion on short-range correlations as revealed by neutron diffraction, which included interchain correlations.

C. Magnetic measurements

Sufficiently above the ordering temperature, $\chi(T)$ has been fitted to the equation $\chi(T) = C/(T - \Theta_W) - \chi_0$. The inclusion of χ_0 corresponds to a correction for the temperature-independent core diamagnetic susceptibility whose value was less than 10^{-4} emu/mol/Oe for all samples. As can be seen from Fig. 8, the magnetic susceptibility (after subtracting the χ_0 correction), exhibits a typical Curie-Weiss behavior at high temperatures. The paramagnetic temperature Θ_W, Curie constant C, and effective magnetic moments μ_{eff} were derived by fitting the experimental data for temperatures larger than 40 K. The refined values are listed in Table V, which shows their evolution with composition. The paramagnetic temperature Θ_W is higher for the Ni-rich side of the solid solution and decreases for large Fe content, but its behavior at intermediate compositions is not clearly defined. Its relatively low values may be taken as indicative of a balance between ferro and antiferromagnetic exchange interactions. Another noticeable feature is that the Θ_W values are positive along the whole series, as can be seen in Table V, reflecting the dominance of ferromagnetic exchange interactions along the chains.
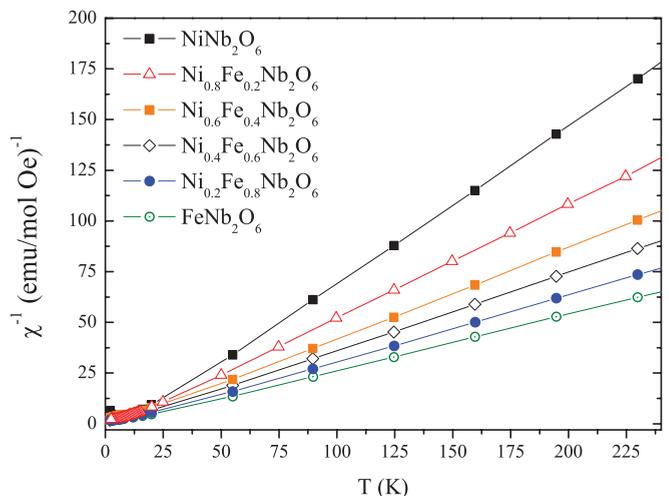
FIG. 8. (Color online) Thermal evolution of the inverse susceptibility for the series $Ni_xFe_{1-x}Nb_2O_6$. Fittings of the high-temperature part with the Curie-Weiss law gives the parameters listed in Table V.

The slope of the linear part of the reciprocal susceptibility in Fig. 8 decreases upon increasing Fe content. This indicates an increase of the mean effective magnetic moment, in agreement with the larger spin of Fe^{2+} with respect to Ni^{2+}. Nevertheless, the effective-moment values, listed for different compositions in Table V, are larger than the spin-only contribution, which is expected in view of the distorted octahedral environment of the magnetic ions.

An isothermal magnetization curve recorded at 3 K for $NiNb_2O_6$ powder sample is plotted in the top panel of Fig. 9. The most interesting feature is the presence of a clearly visible change of slope slightly above $\mu_0 H = 1$ T, followed by a weak hysteresis. We interpret this as resulting from the field-induced ferromagnetic alignment of the zigzag chains as the applied magnetic field becomes large enough to overcome the weak AF interchain interactions, thus inducing an antiferromagnetic to ferromagnetic transition. Similar behavior has been reported for isotype compounds.[2] This transition does not appear in the isothermal magnetization curves recorded for $Ni_{0.2}Fe_{0.8}Nb_2O_6$, gathered in the bottom panel of Fig. 9. Unlike for pure $NiNb_2O_6$, it shows a strong increase of the magnetization with field at low temperatures, indicating that the field necessary to induce a ferromagnetic alignment between the chains is very small. The same behavior is observed for the compounds with $x = 0.4$, 0.6, and 0.8, once more confirming the indications of absence of magnetic order already obtained from neutron-diffraction and specific-heat measurements.

TABLE V. Composition dependence of the magnetic properties of the $Ni_xFe_{1-x}Nb_2O_6$ compounds in the paramagnetic state.

x	θ_W (K)	C (emu K/mol Oe)	μ_{eff} (μ_B)
1	9.96	1.36	3.30
0.80	7.2	1.84	3.84
0.60	8.1	2.26	4.25
0.40	6.4	2.68	4.63
0.20	7.2	3.14	5.01
0	6.6	3.67	5.42

FIG. 10. (Color online) ^{57}Fe Mössbauer spectra recorded at room temperature on the indicated compounds of the $Ni_xFe_{1-x}Nb_2O_6$ series. The points are the experimental data and the line is the corresponding fitting.

there. This involves an interchain exchange $J_\perp$, which is to be viewed as an average of the J_1 and J_2 couplings shown in Fig. 6, and is obtained using the known values the Néel temperature T_N. It is interesting to notice that the values of J_0 extracted here from the susceptibility data are comparable to those determined from the specific-heat measurements (see Table IV), but somewhat lower. This may be understood as an effect of the interchain AF interactions, which are not frustrated in the paramagnetic phase due to the presence of the applied (measuring) field, which induces parallel average spins on all sites.

D. Mössbauer data

In natural (and, consequently, partially ordered) columbite samples,[27–29] the Mössbauer spectra present two quadrupole doublets (ΔE_Q), both attributed to Fe^{2+} in different octa-hedrally coordinated sites. The site assignment is justified because the quadrupole splitting is inversely correlated with the octahedral distortions.[29] Indeed, it has been shown[24,30] that the FeO_6 octahedra are less distorted than the NbO_6 ones. We consequently attribute the single doublet observed here ($\Delta E_Q \sim 1.8$ mm/s) to Fe^{2+} in the more distorted FeO_6 octahedra. The absence of any other doublet proves the ordering of the iron atoms during the synthesis, occupying only A sites in the AB_2O_6 structure. Typical Mössbauer spectra recorded at room temperature are presented in Fig. 10 for the $x = 0.2$, 0.4, and 0.8 samples.

The hyperfine parameters derived from the fitting of the Mössbauer spectra recorded for three samples are listed in Table VI. It is clear that the obtained values for the isomer shift and the quadrupole splitting are typical of Fe-type octahedral sites, indicating the exclusive presence of iron in Fe^{2+} state on this octahedral positions in the investigated samples. The obtained values can be compared to those reported earlier for the pure $FeNb_2O_6$ compound.[31] The obtained quadrupole splittings are similar to those reported at room temperature by Eibschütz *et al*. and slightly larger than what is observed in

FIG. 9. (Color online) (Top) Hysteresis cycle recorded at 3 K for $NiNb_2O_6$ powder with evidence of a metamagnetic transition. (Bottom) Isothermal magnetization curves recorded at the indicated temperatures for the $Ni_{0.2}Fe_{0.8}Nb_2O_6$ compound without any visible indication of magnetic ordering, but with a strong response at low temperature.

As has been done in the case of $CoNb_2O_6$, assuming an Ising type model for the zigzag cation chains and a mean exchange interaction between the chains, a fit of the thermal variation of the magnetic susceptibility can be used to extract the magnetic coupling constants. For the $Ni_xFe_{1-x}Nb_2O_6$ compositions that do not present any long-range ordering, we considered the system as composed of isolated spin chains. The intrachain exchange coupling J_0 was consequently extracted from the known formula[26] for the magnetic susceptibility of a single chain,

$$\chi_0 = \frac{S^2}{T} e^{2S^2 J_0/T}. \quad (4)$$

Values of J_0 were found to vary from 1.03 to 2.51 K for $x = 0.2$ and 0.8, respectively. The values determined for each composition are summarized in Table IV together with those of the reference Ni and Fe compounds. The parameters for $FeNb_2O_6$ have already been reported in Ref. 24, and those for $NiNb_2O_6$ were determined by the procedure described

TABLE VI. Hyperfine parameters derived from fittings of the room-temperature Mössbauer spectra recorded for three samples of the $Ni_xFe_{1-x}Nb_2O_6$ compounds. The isomer shift (IS) is given relative to that of elemental α-Fe.

Sample	EQ (mm/s)	IS (mm/s)	Linewidth (mm/s)
$Ni_{0.2}Fe_{0.8}Nb_2O_6$	1.79 (0.01)	1.15 (0.01)	0.27 (0.01)
$Ni_{0.4}Fe_{0.6}Nb_2O_6$	1.82 (0.01)	1.11 (0.01)	0.27 (0.01)
$Ni_{0.6}Fe_{0.4}Nb_2O_6$	1.86 (0.01)	1.15 (0.01)	0.28 (0.01)

ordered natural (Fe,Mn)-containing columbite,[29] where values of $\Delta E_Q \sim 1.8$ mm/s are obtained.

In the samples studied here, the linewidth after heat treatment is typically of 0.275 mm/s, a value close to the instrumental resolution of 0.26 mm/s, as determined from the α-Fe foil reference used for calibration of the Mössbauer spectrometer. It is worth to remark that the isomer shift and the linewidth do not show a clear evolution with composition. On the contrary, the quadrupole splitting is found to exhibit a continuous increase upon increasing the Ni content. Such evolution could be due to two main origins: a change of the spin-orbit coupling or an increase of the distortion of the octahedron surrounding the Fe^{2+} ions. Taking into account the nearly identical linewidth along the series, a modification of the spin-orbit coupling is the most probable origin of the observed change in the quadrupole splitting. Indeed, the importance of spin-orbit coupling was already pointed out by Eibschutz *et al.*[31] in their study of the crystal field in $FeNb_2O_6$.

IV. CONCLUSIONS

We now summarize the main results reported here. Fe for Ni substitution in $NiNb_2O_6$ is found to preserve the orthorhombic crystal structure and to induce a continuous increase of the lattice volume. The expansion occurs mainly along the *a* and *b* axes.

Investigation of the magnetic properties shows that the $(Fe,Co)Nb_2O_6$ compounds exhibit particularly small

paramagnetic temperature. In spite of the fact that the two "pure" compounds $FeNb_2O_6$ and $NiNb_2O_6$ are magnetically ordered at low temperature, chemical disorder induces a loss of long-range magnetic order in the $Ni_xFe_{1-x}Nb_2O_6$ series for $x = 0.2$, 0.4, 0.6, and 0.8. Nevertheless, the dominant exchange interactions in the system are ferromagnetic, occurring inside the zigzag chains along the *c* axis, and magnetization isotherms recorded at 2 K show that a small applied magnetic field can induce ferromagnetic-like behavior, reflecting the induced ordering within the chains. The paramagnetic Curie-Weiss temperatures are positive throughout the series, also bearing witness to the fact that the ferromagnetic interactions within the cation chains are dominant.

Neutron powder diffraction shows that for $x = 0.2$, 0.4, 0.6, and 0.8 no magnetic order is established down to 1.7 K. For $x = 0.2$, measurements were performed down to 400 mK without observation of long-range magnetic order, but short-range correlations of magnetic origin are implied by the presence of a diffuse neutron scattering broad bump. Fitting of the diffuse magnetic signal reveals the existence of ferromagnetic correlations within the zigzag chains, whereas interchain correlations are found to be antiferromagnetic. These short-range correlations, clearly visible in the neutron-diffraction patterns, are also indicated by the specific-heat behavior at very low temperatures, which slightly departs from the single-chain behavior. In conclusion, considering the question of whether the Ising chains become isolated by frustration in the $Ni_xFe_{1-x}Nb_2O_6$ compounds, the answer is yes, but weak short-range correlations remain.

*Corresponding author: olivier.isnard@grenoble.cnrs.fr

[1]C. Heid, H. Weitzel, F. Bourdarot, R. Calemczuk, T. Vogt, and H. Fuess, J. Phys.: Condens. Matter **8**, 10609 (1996).

[2]C. Heid, H. Weitzel, P. Burlet, M. Bonnet, W. Gonschorek, T. Vogt, J. Norwig, and H. Fuess, J. Magn. Magn. Mater. **151**, 123 (1995).

[3]S. Kobayashi, S. Mitsuda, and K. Prokes, Phys. Rev. B **63**, 024415 (2000).

[4]Y. Zhou, M. Lu, Z. Qiu, A. Zhang, Q. Ma, H. Zhang, and Z. Yang, Mater. Sci. Eng. B **140**, 128 (2007).

[5]J. Ye, Z. Zhou, and A. Matsushita, Int. J. Hydrogen Energy **28**, 651 (2003).

[6]R. C. Pullar, C. Vaughan, and N. McN Alford, J. Phys. D: Appl. Phys. **37**, 348 (2004).

[7]R. C. Pullar, J. Am. Ceram. Soc. **92**, 563 (2009).

[8]R. W. G. Wyckoff, *Crystal Structure* (Wiley, New York, 1965).

[9]A. I. Zaslavsky, Y. D. Kondrashev, and S. S. Tolkachev, Dokl. Akad. Nauk SSSR **75**, 559 (1950).

[10]H. Weitzel, Anorg. Allg. Chem. **380**, 119 (1971).

[11]I. Yaeger, A. H. Morrish, and B. M. Wanklyn, Phys. Rev. B **15**, 1465 (1977).

[12]I. Yaeger, A. H. Morrish, B. M. Wanklyn, and B. J. Garrard, Phys. Rev. B **16**, 2289 (1977).

[13]A. Barlet, J. C. Genna, and P. Lethuillier, Cryogenic **31**, 801 (1991).

[14]J. Rodriguez-Carvajal, Physica B **192**, 55 (1993).

[15]L. B. McCusker, R. B. Von Dreele, D. E. Cox, D. Louer, and P. Scardi, J. App. Cryst. **32**, 36 (1999).

[16]V. F. Sears, Neutron News **3**, 26 (1992).

[17]G. M. Bancroft, *Mössbauer Spectroscopy. An introduction for Inorganic Chemists and Geochemists* (McGraw-Hill, London, 1973).

[18]G. J. Long, T. E. Cranshaw, and G. Longworth, Mössbauer effect Ref. Data **6**, 42 (1983).

[19]E. F. Bertaut and P. Burlet, Solid State Commun. **5**, 279 (1967).

[20] A. Wiedenmann, P. Burlet, H. Scheuer, and P. Convert, Solid State Commun. **38**, 129 (1981).

[21] J. E. Greedan, J. N. Reimers, C. V. Stager, and S. L. Penny, Phys. Rev. B **43**, 5682 (1991).

[22] I. Mirebeau, A. Apetrei, J. Rodriguez-Carvajal, P. Bonville, A. Forget, D. Colson, V. Glazkov, J. P. Sanchez, O. Isnard, and E. Suard, Phys. Rev. Lett. **94**, 246402 (2005).

[23] S. Kobayashi, S. Mitsuda, M. Ishikawa, K. Miyatani, and K. Kohn, Phys. Rev. B **60**, 3331 (1999).

[24] P. W. C. Sarvezuk, E. J. Kinast, C. V. Colin, M. A. Gusmão, J. B. M. da Cunha, and O. Isnard, Phys. Rev. B **83**, 174412 (2011).

[25] S. Lee, R. K. Kaul, and L. Balents, Nat. Phys. **6**, 702 (2010).

[26] D. C. Mattis, *The Theory of Magnetism* (Harper and Row, New York, 1965).

[27] V. D. Mello, L. I. Zawislak, J. B. Marimon da Cunha, E. J. Kinast, J. B. Soares, and C. A. dos Santos, J. Magn. Magn. Mater. **196-197**, 846 (1999).

[28] S. C. Tarantino, M. Zema, M. Pistorino, and M. C. Domeneghitti, Phys. Chem. Minerals **30**, 590 (2003).

[29] E. J. Kinast, O. Isnard, J. B. M. da Cunha, M. A. Z. Vasconcellos, and C. A. dos Santos, J. Appl. Cryst. **44**, 738 (2011).

[30] D. T. Griffen and P. H. Ribbe, N. Jb. Miner. Abh. **137**, 54 (1979).

[31] M. Eibschütz, U. Ganiel, and S. Shtrikman, Phys. Rev. **156**, 259 (1967).